Parry arc: a polarization lidar, ray-tracing, and aircraft case study

Kenneth Sassen and Yoshihide Takano

Using simple ray-tracing simulations, the cause of the rare Parry arc has been linked historically to horizontally oriented columns that display the peculiar ability to fall with a pair of prism faces closely parallel to the ground. Although we understand the aerodynamic forces that orient the long-column axis in the horizontal plane, which gives rise to the relatively common tangent arcs of the 22° halo, the mechanism leading to the Parry crystal orientation has never been resolved adequately. On 16 November 1998, at the University of Utah Facility for Atmospheric Remote Sensing, we studied a cirrus cloud producing a classic upper Parry arc using polarization lidar and an aircraft with a new high-resolution ice crystal imaging probe. Scanning lidar data, which reveal extremely high linear depolarization ratios δ a few degrees off the zenith direction, are simulated with ray-tracing theory to determine the ice crystal properties that reproduce this previously unknown behavior. It is found that a limited range of thick-plate crystal axis (length-to-diameter) ratios from ~0.75 to 0.93 generates a maximum $\delta \approx$ 2.0–5.0 for vertically polarized 0.532-μm light when the lidar is tilted 1°–2° off the zenith. Halo simulations based on these crystal properties also generate a Parry arc. However, although such particles are abundant in the *in situ* data in the height interval indicated by the lidar, one still has to invoke an aerodynamic stabilization force to produce properly oriented particles. Although we speculate on a possible mechanism, further research is needed into this new explanation for the Parry arc.

OCIS codes: 010.0010, 010.2940, 010.3640, 290.1350.

1. Introduction

Prolonged scientific inquiry into the causes of atmospheric optical phenomena has served to promote major advances in the fundamental laws of physics, including refraction, polarization, and interference. In an attempt to comprehend halos and arcs in cirrus clouds, the basic hexagonal shapes and fall attitudes of ice crystals were deduced through simple ray-tracing scattering simulations long before they could be examined under the microscope.[1,2]

One of the rarer arcs was first sketched by that indomitable polar explorer Sir William Edward Parry (1790–1855) while searching for the Northwest Passage.[3] References 1 and 2 provide copies of the original drawing of this complex optical display. Parry's arc was noted as a suncave arc overlying the upper tangent arc rising from the 22° halo, or as Tricker[1] has put it, "The Parry arc . . . occupies the position between the horns of the upper arc of contact to the halo of 22°, as was indicated by Parry." Once the general explanation for this arc was provided by Hastings[4] and after Wegener[5] simulated its geometry, Putnins[6] numerically discovered a set of other arcs that should also be caused by the same crystal orientation. The explanations for the various phenomena sketched on this occasion by Parry require increasingly rigid conditions for uniformly orienting ice crystals in space. The 22° halo merely needs more or less randomly oriented hexagonal crystals, whereas in the tangent arc column crystals must align their long *c* axis in the horizontal plane, but the Parry arc further requires that such columns fall with a pair of prism faces closely parallel to the ground, the so-called doubly oriented ice prism.

The ability of an ice crystal to orient during fall is a well-known consequence of aerodynamic drag forces, which, as functions of air density, and particle shape, density, and fall speed, tend to align the particle with its maximum cross section orthogonal to

K. Sassen (ksassen@met.utah.edu) is with the Department of Meteorology, University of Utah, 135 South 1460 East, Room 819 WBB, Salt Lake City, Utah 84112-0110. Y. Takano is with the Department of Atmospheric Science, University of California, Los Angeles, Los Angeles, California 90095.

Received 5 June 2000; revised manuscript received 25 September 2000.

0003-6935/00/366738-08$15.00/0

the direction of flow (i.e., gravity). Primarily, within the troposphere it is the ice crystal size that determines whether it will orient uniformly. Experimental evidence indicates that the crystals must be approximately 100–200 μm in maximum dimension to orient stably in the horizontal plane, whereas particles larger than ~1 mm will tend to oscillate about the preferred orientation and lose the strict horizontal alignment.[7] The latter effect is related to the shedding of turbulent eddies in the wake of rapidly falling particles.

Unfortunately for the common Parry arc explanation, there is no mechanism that can convincingly account for the peculiar doubly oriented requirement. Rather, for a horizontally oriented symmetrical ice column there should be no preference for a fall pattern favoring the alignment of any prism face: Although commonly two-dimensionally oriented in space, columns should not display such a three-dimensional (3-D) preference. Thus the simple theoretical model of Parry-oriented column crystals cannot be satisfied until the mechanism promoting 3-D orientation is found.

In this paper we exploit a data set derived from an advanced remote sensing and coordinated aircraft case study of a cirrus cloud layer that serendipitously generated a classic upper Parry arc. The combination of scanning polarization lidar, photographic, and *in situ* particle imaging data provides a unique portrait of the content of a Parry arc-producing cloud. Importantly, we apply ray-tracing simulations to explain the strong scattering anisotropy observed in the lidar data, from which an unexpected finding regarding particle shape is deduced.

2. Remote Sensing Findings

The Facility for Atmospheric Remote Sensing (FARS) supports a variety of active and passive instruments for cloud and aerosol research.[8] FARS has two lidars and a *W*-band Doppler radar that are equipped with polarization diversity, in which linear polarized pulses are emitted and the backscatter is collected in the planes of polarization orthogonal and parallel to that of the source. The ratio of these two signals, after correcting for receiver channel gains, yields the linear depolarization ratio or δ value. As reviewed recently,[9] lidar depolarization measurements in clouds provide important insights into the shapes and orientations of the particles present. To illustrate, we begin by presenting data collected over the case study period with our turnkey cloud polarization lidar (CPL), a 0.1-Hz ruby laser (0.694-μm) dual-channel system with a 7.5-m range resolution.

Figure 1 shows height versus time displays of range-normalized attenuated backscattering and linear depolarization ratios obtained on 16–17 November 1998. At the top of the figure are a series of all-sky fish-eye photographs as the optical phenomena evolved, and on the right-hand side is the local temperature sounding for 0000 UTC on 17 November 1998. The returned energy display, which is equivalent to an advected distance of ~700 km at the 38.5-m s^{-1} mean cirrus level wind speed, is not unusual for mid-latitude cirrus clouds. The ~5.0-km-deep cloud extends to the tropopause height and contains evidence for near-cloud-top-generating regions, which sporadically produce deep ice particle fall streaks that serve to maintain the cloud layer. The depolarization display is unusually colorful (i.e., variable) with regard to most of the mid-latitude cirrus we have studied over the past 13 years at FARS, but is more common with halo-producing cirrus layers, which tend to produce relatively lower δ values.[10] By occasionally tipping the CPL a few degrees off the zenith direction, we verified that the areas displaying the $\delta < 0.15$ contained horizontally oriented planar ice crystals. The specular reflections from such crystals, if present in sufficient numbers in relation to coexisting particles,[9] can generate near-zero δ with a zenith lidar.

The polarization diversity lidar (PDL)[11] is a considerably more advanced device based on a Nd:YAG laser transmitting at 10 Hz in both the 1.06 and the frequency-doubled 0.532-μm wavelengths. Each color has its own telescope and dual-channel receiver package, which, along with the transmitter and an *X*-band radar eye-safety system, are mounted on a scannable optical table. The data-acquisition system allows four-channel 10-Hz data recording with a maximum range resolution of 1.5 m, making this a uniquely high-resolution scanning cloud lidar. The two PDL 0.532-μm data displays in Fig. 2 consist of single ±10° range–height scans from the zenith direction, obtained during two periods that show an elevation angle dependence in depolarization. These scans correspond to times that the Parry arc was absent [Fig. 2(a)] and near its most developed [Fig. 2(b)] (see the date- and time-stamped fish eyes in Fig. 1). Figure 3 provides a wide-angle view of the colorful optical phenomena present near the time that the scan in Fig. 2(b) was collected.

The lidar scan in Fig. 2(a) depicts the situation for a cloud containing a mixture of horizontally oriented plate crystals and those of different shapes and orientations. The zenith-returned energy peak and δ-value minimum are common for such conditions, although the approximately ±1.0° width of these features is unusually narrow for most cirrus, except for those producing brilliant halos and arcs.[10,12] This points to the requisite condition for the crystals causing vivid displays to have small wobble angles, as can also be demonstrated through halo simulations.[13] That a mixture of properly oriented and other particles was present is indicated by the relatively high zenith depolarization, which shortly afterward produced near-zero δ values (see Fig. 1). Compared with the angular depolarization patterns predicted with ray tracing when only oriented plates are present,[14] the off-zenith measurements differ significantly because the relatively weak plate backscattering is overwhelmed by contributions from the other crystals that are present. The dissimilar lidar scan in Fig. 2(b), on the other hand, is unique in our experience. Although, as before, lower δ values oc-

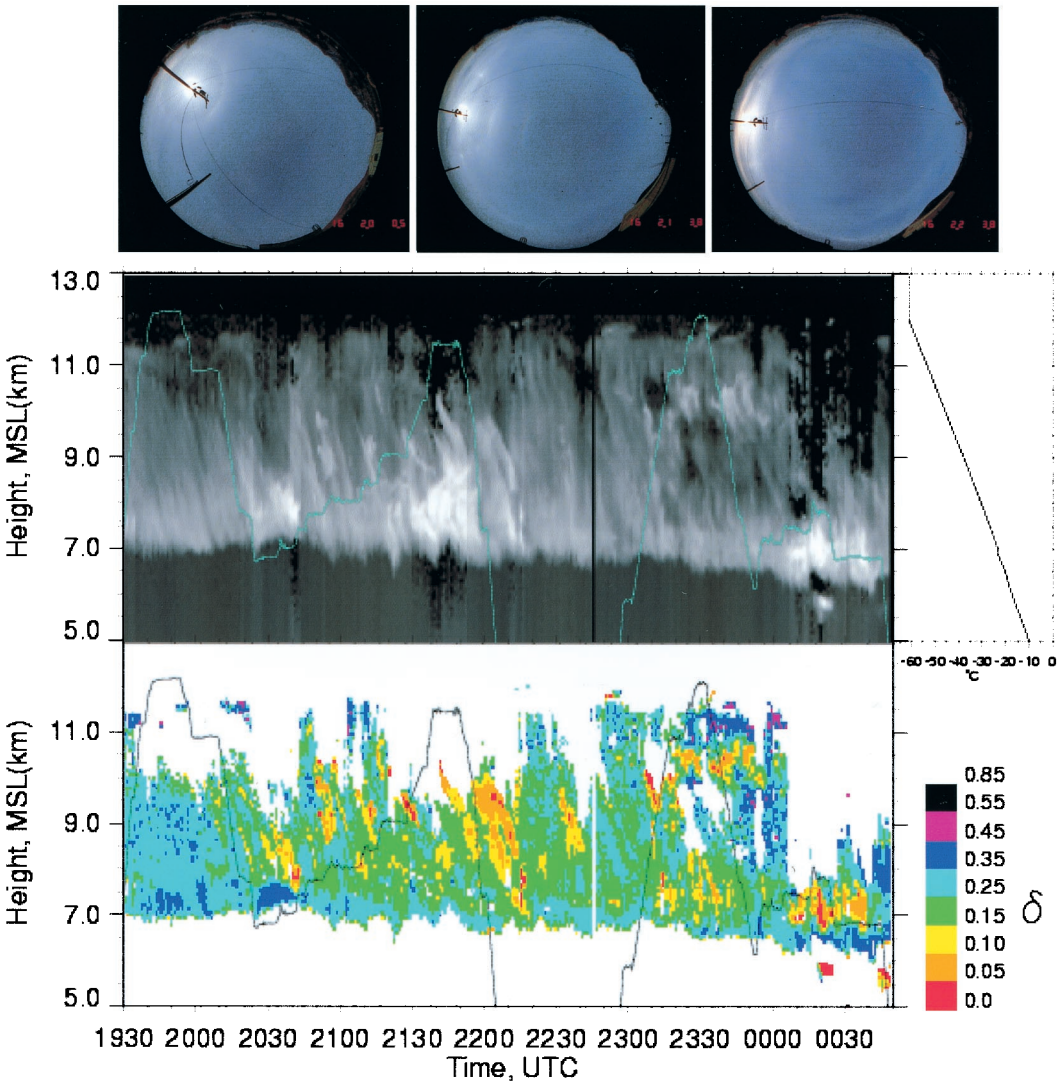

Fig. 1. Height versus time displays of CPL (0.694-μm) relative backscattering (middle, based on a logarithmic gray scale) with local temperature profile and linear depolarization ratios (with the color δ scale on the right-hand side) for the cirrus studied on 16 November 1998. The altitude of the supporting Lear jet mission in the vicinity of FARS is superimposed over the lidar data. Representative fish-eye photographs obtained at the indicated date and times in UTC are shown at the top. MSL, mean sea level.

cur close to the zenith, between ~1.0° and 2.0° the depolarization is extremely high and approaches unity. We speculate that this highly anisotropic depolarization pattern is attributable to the dominant ice crystal shape and orientation responsible for the Parry arc.

3. Ray-Tracing Simulations

Equipped with the knowledge of this unique angular scattering behavior, we applied geometric ray-tracing models to reproduce the lidar and photographic data and thus constrain the cirrus cloud microphysical conditions associated with the rare Parry arc. First we simulated the polarization lidar scan in Fig. 2(b), and then used our findings to determine if we could also reproduce the optical displays that were present. The model used for computations of the linear depolarization ratio is described in Takano and Jayaweera[14] and Takano and Liou.[15] We employ the model of a regular solid hexagonal ice crystal with a refractive index of $1.31172 - i2.618 \times 10^{-9}$ at the 0.532-μm wavelength. For a specified off-zenith scanning angle α, the azimuth angles β of 30.0° and 30.5° are taken into account for the Parry orientation. Rays scattered from 179° to 180° angles are counted as backscattered rays, and, roughly speaking, the crystal wobble angle can be regarded as 0.5°. Because there is almost no absorption by ice in this case, only a relative value of the crystal aspect ratio $L/2a$ (where L is the crystal c-axis length and a is the maximum radius) is specified in our computations. $L/2a$ was varied over a large range of values including those for thick-plate ($L/2a < 1.0$) and column ($L/2a > 1.0$) crystals.

In our simulations we assume the veracity of the basic Parry crystal orientation, which is shown in Fig. 4 along with the traditional view of the solar scattering geometry responsible for the arc.[13] The

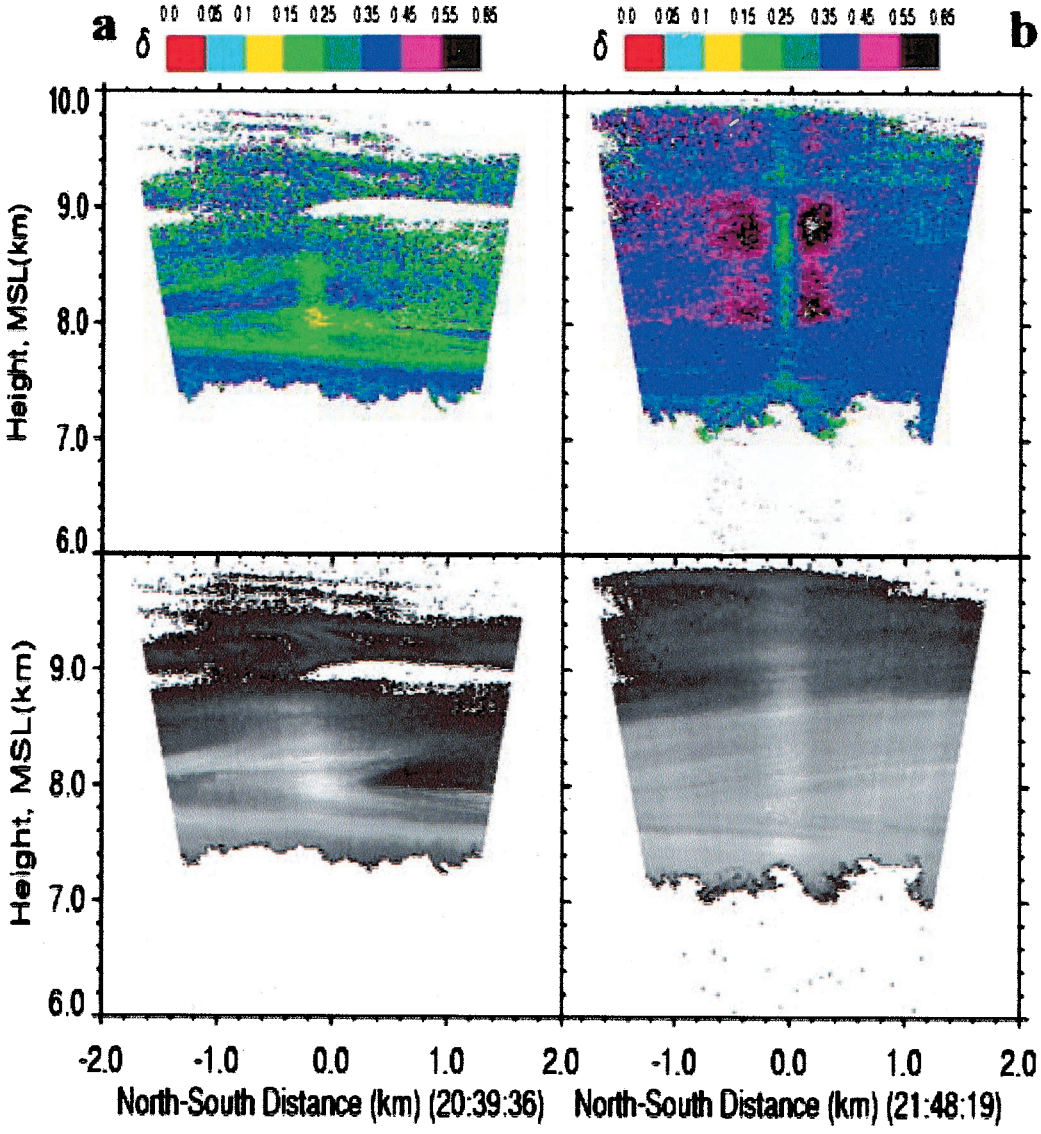

Fig. 2. Comparison of PDL (0.532-μm) ±10° zenith elevation angle scans begun at the indicated times (in UTC) in terms of δ values (top) and relative returned energy obtained at a 1.0°-s^{-1} scan rate. The scan in b was obtained when the Parry arc was at its maximum brilliance. Note that the slight asymmetry in the δ patterns is probably the result of a small error in the level of the truck-mounted PDL system. MSL, mean sea level.

Parry arc ray path enters the long-column crystal through the top prism face and exits through an alternate prism face. However, Parry-oriented long columns could not reproduce the lidar depolarization measurement in Fig. 2(b): Only a narrow range of thick-plate axial ratios, which were nearly equidimensional, could. The appropriate model-predicted ray path through a Parry-oriented $L/2a = 0.833$ thick plate is shown in Fig. 5 in side and top views, in terms of the lidar geometry. The ray of laser light at $\alpha = 2.0°$ enters the crystal through a basal face (dashed line at right, top view) and suffers a number of refractions and internal reflections until it reemerges into the backscattering direction. Oddly, as it exits into the backscattering direction the remaining energy is recycled through the same internal path.

Figures 6(a) and 6(b) shows the linear depolarization ratio δ_v and the relative backscattered intensity[14] $M = [M^{(2)} + M^{(4)}]$ for vertically polarized 0.532-μm light as functions of the off-zenith scanning angle and the crystal aspect ratio. When α is less than 0.5°, δ_v is ~0 but M is quite high because of specular reflection at the bottom prism face. When $\alpha > 0.5°$, δ_v becomes larger because of the rays illustrated in Fig. 5, whereas M decreases because of the absence of the strong specular reflection. This border value of $\alpha = 0.5°$ results from the assumed wobble angle of 0.5°, but the actual angle would be more vague (say, 0.5°–1.0°). For $\alpha > 2°$, δ_v approaches zero and M again becomes high. This is because the plane skew rays and spatial skew rays contributing to backscattering[14] are incident, respectively, on the bottom prism face and the lower sloping prism faces

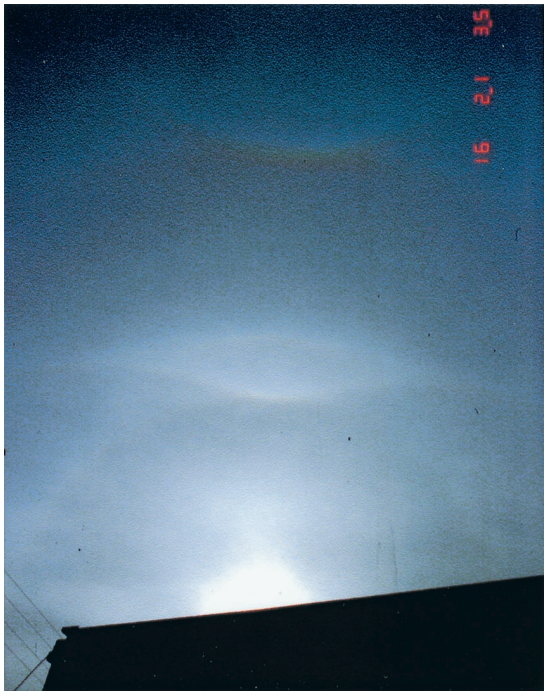

Fig. 3. Photograph taken with a 24-mm wide-angle lens at the indicated time of the vivid Parry arc and tangent arc combination plus the circumzenith arc. Note the weak colorization on the inner Parry arc (middle arc).

and can be reflected internally off the basal face. Even the spatial skew rays give rise to near-zero values of δ_v because almost no rotation of the incident polarization plane occurs.

Thus, to reproduce the lidar scan of Fig. 2(b), the generation of the abnormally strong δ_v from $\alpha \approx 1°$–$2°$ [Fig. 6(a)] must be weighed against the corresponding relative backscattered intensities [Fig. 6(b)]. Although the highest δ_v correspond to the lowest M, various M and δ_v can contribute to an observable depolarized lidar signal between $\alpha \approx 1°$–$2°$, depending on the thick-plate axis ratio. Additional factors, however, are the degree to which the crystals are permitted to wobble from the horizontal plane in the

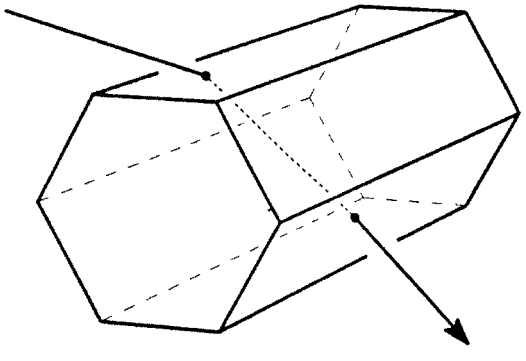

Fig. 4. Traditional view of the ray path responsible for the Parry arc shown in solar scattering geometry (after Ref. 13). The long-solid-column crystal must fall with a pair of prism faces strictly parallel to the ground.

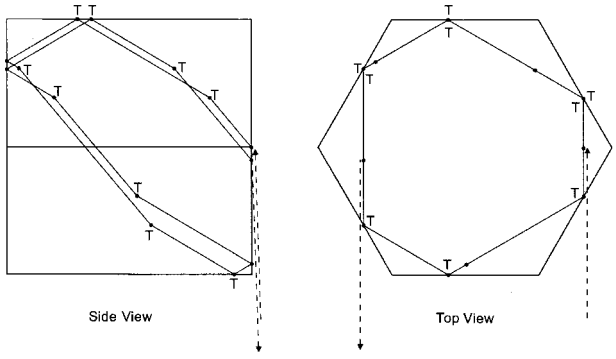

Fig. 5. Schematic views of the predicted ray path through a $L/2a = 0.833$ Parry-oriented thick-plate crystal responsible for the strongly depolarized backscattering at $\alpha = 2°$, shown in terms of the lidar scattering geometry. The dots mark the locations of reflections and internal refractions off the basal and prism faces and T denotes total internal reflection.

simulations and the relative number of properly oriented versus other crystals present in the lidar scattering volume. For example, if the crystals were allowed to wobble $\pm 2.0°$ from the horizontal, the strengths of the backscattering features would over-

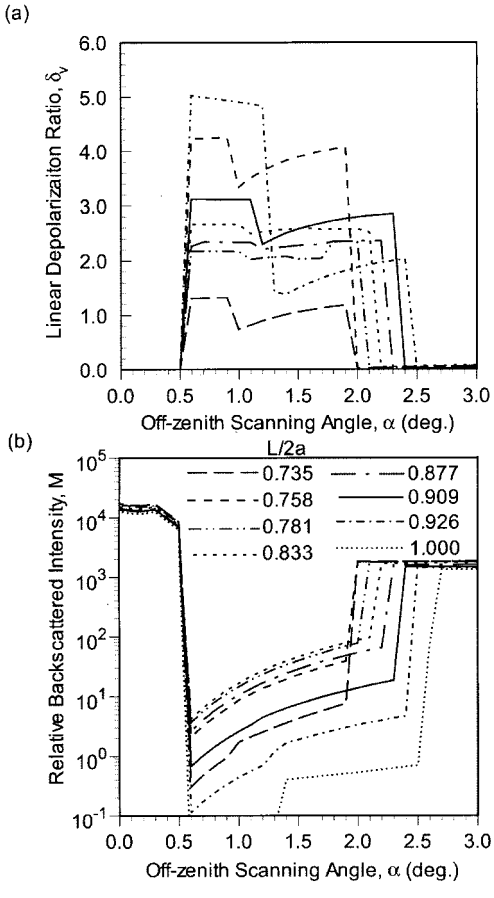

Fig. 6. Plots of (a) δ_v values and (b) relative lidar backscattering M as a function of the off-zenith scanning angle α and the identified thick-plate axis ratios $L/2a$ (see inserted key in (b). δ_v values for $L/2a = 1.0$ are too low in (a) to be discerned in the figure.

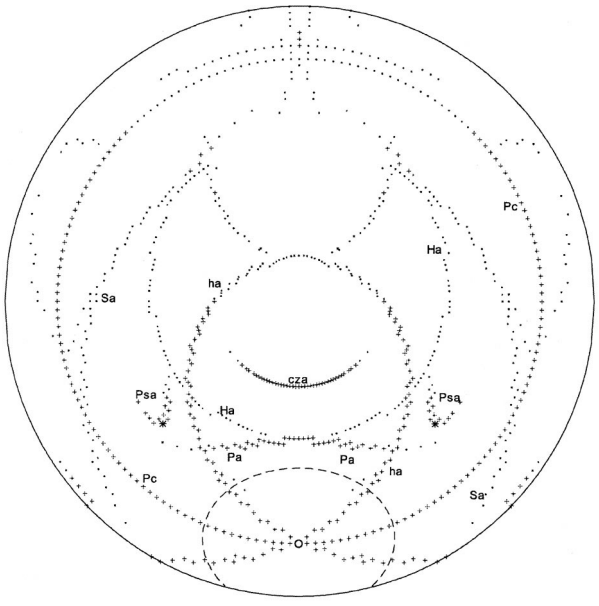

Fig. 7. Zenith-centered all-sky simulation of the optical phenomena generated by Parry-oriented thick-plate crystals ($L/2a$ = 0.833) for a solar elevation angle of 17° and a 0.532-μm wavelength, where ▪, +, and ∗ represent the log 0, 1, and 2 relative scattering intensity, respectively. The Sun position is indicated by the open circle near the bottom, and the position of the 22° halo is indicated by the dashed circle. The inserted abbreviations for the observed arcs are defined in the text.

lap and be spread out. It is also clear that a variety of crystal types and sizes normally coexist in cirrus clouds, which further dilutes the strengths of the scattering patterns that are simulated when a uniform crystal assemblage is assumed.

These ray-tracing simulations of backscatter depolarization indicate that it is only near-equidimensional Parry-oriented thick-plate crystals that could be responsible for the lidar scan data. At the same time, as shown in the halo prediction based on such a crystal model in Fig. 7, these particles are also capable of generating the observed optical phenomena. For these simulations using regular solid hexagonal crystals, we adopted the Takano and Liou[16] model. Although the crystal wobble angle is assumed to be 0°, because of the coarse angular resolution (2°) used, the halo pattern produced is similar to that for a 0.5° wobble angle. A comparison of this prediction to the photographs in Figs. 1 and 3, and to sketches of faint arcs recorded in field notes, reveals that most of the lesser arcs were not observed during the study period. When we considered first the optics formed from Parry-oriented thick plates, a bright and colored suncave Parry arc (labeled Pa in Fig. 7), circumzenith arc (cza), and parhelic circle (pc) were observed, as well as a vague Parry supralateral arc (Psa). Faint, incomplete arcs that could represent the heliac (ha), subhelic (sa), and Hastings (Ha) arcs were noted. However, other features from singly oriented (horizontal) columns like the upper and lower tangent arcs to the 22° halo and weak supralateral arcs were identified. Finally, intense parhelia from horizontally oriented thick plates, and of course the common 22° halo from more or less randomly oriented crystals, also are represented clearly in the photographs. It now remains to be determined if such particles, and especially the peculiarly oriented thick-plate crystal, are preserved in the *in situ* ice particle data set.

4. In Situ Findings

This FARS case study was supported by a Lear jet cirrus cloud research mission from Stratton Park Engineering equipped with standard particle measuring system ice crystal probes, plus a cloud particle imager using a uniquely high-resolution (~5-μm) laser-imaging device.[17] The aircraft height versus time trace during its mission in the vicinity of FARS is superimposed on the CPL returned energy height–time displays in Fig. 1.

Given that the ray-tracing experiments have indicated an approximately equidimensional hexagonal shape, an effort can be made to determine if such particles were measured *in situ* at the lidar-determined heights and times. In addition, to maintain stable fall attitudes at cirrus altitudes[7] we assume that the crystals must be larger than ~150 μm and be essentially solid so as not to interfere with internal scattering. However, the microphysical content of cirrus clouds is normally quite mixed with regard to ice crystal habit because of the contributions of factors such as new particle generation, sedimentation, turbulent mixing, and aggregation.[18] Thus *in-situ*-derived crystal compositions must be scrutinized carefully to reveal if the proper subset of particles contributing to a particular display is present.

Because anomalously strong lidar depolarization was measured between 8.0- and 9.0-km altitude (−30 °C to −40 °C) during a series of consecutive lidar scans just prior to 2150 UTC, and the brightest Parry arc lasted from 2130 to 2150 UTC, the flight track in Fig. 1 indicates that the aircraft came closest to sampling this cloud region during a spiral descent from 2150 to 2200 UTC. Figure 8 shows a number of selected images from the cloud particle imager, which demonstrate that the predicted ice crystal type existed in the appropriate region of the cloud. This subset of the crystals, which were nearly all solid, clearly satisfies the need for nearly equidimensional particles, and several appear to display the proper 3-D orientation. Note that, depending on the viewing geometry, it may be difficult to determine the precise particle shape and orientation, and some disturbance of the fall attitude can occur from aerodynamic forces caused by the aircraft shell or the probe. Of course, as expected, other particle types are present, the majority of which are less than ~50-μm and are of an indeterminent form. Of the larger 200–500-μm particles, many are not identified easily but resemble spatial particles comprised of columns and sector planes, along with some long columns and structured plates. The particle types shown in Fig.

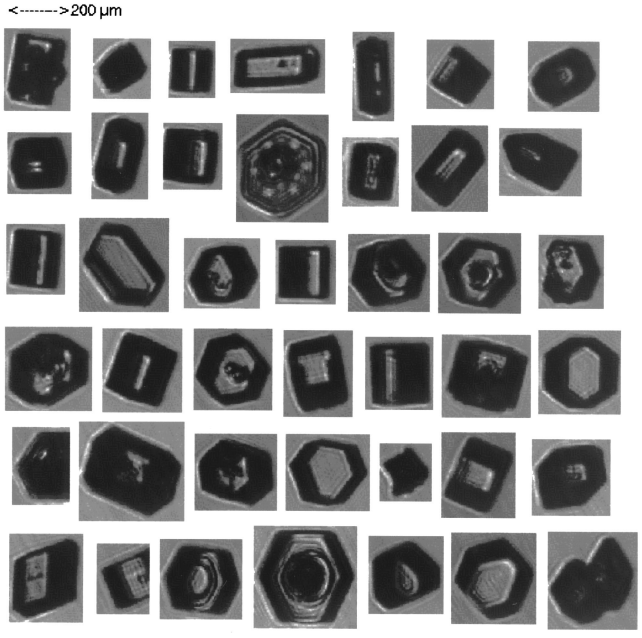

Fig. 8. Selected ice crystal images from the *in situ* cloud particle laser-imaging probe showing the predicted shapes collected between 2156:07 and 2159:53 during a spiral descent from 8.0 to 9.0 km, following the lidar scan and optics photograph of Figs. 2(b) and 3. The top shows the scale for a 200-μm particle. Note the tendency for the crystal axis ratios to decrease with descent, from top left to bottom right.

8, however, were common among the large particles at this time and place during the mission.

5. Conclusions

Based on the combined evidence from a remarkable new *in situ* probe and a ray-tracing inversion of polarization lidar scans obtained in a cirrus cloud, we conclude that, at least in this case, a rare Parry arc was generated by nearly equidimensional thick-plate crystals displaying the so-called Parry orientation. We should point out that typically such particles are also present in the surface ice crystal samples collected by Tape[13] in Antarctica during complex optical displays that included the Parry arc. Of course other crystal shapes were present, including some of the long solid columns previously regarded as the cause of the Parry arc. Regardless of the crystal axial ratio, however, one is confronted ultimately with explaining the tendency for some particles to fall with a pair of prism faces strictly parallel to the ground.

It may be that the necessary condition for double orientation is simply a consequence of how the thick-plate or short-column crystal adjusts its fall attitude in switching from the basic plate to column orientation. In other words, in transitioning between the two stable free-fall modes, it can be hypothesized that unusual aerodynamic forces come into play that lead to 3-D stabilization. Another question is the characteristic axis ratio for which this fall pattern transition occurs. Is it just a coincidence that the unique lidar depolarization scans, which could be reproduced theoretically over only a limited range of axis ratios, have served to reveal it? Such conjecture should be tested with the method of tank experiments by use of appropriate ice crystal models.

There is a final piece of evidence that may have bearing on the issue of rare arc generation, and that is the unusual (i.e., for FARS) nature of the cirrus cloud layer studied on this occasion. As discussed earlier,[12] there seems to be a connection between complex halo–arc displays and the origin of the cirrus. As in earlier cases of rare arcs occurring in mid-latitude cirrus derived from upper-level hurricane outflow,[12,19] the cirrus cloud studied on 16 November 1998 was also of tropical or subtropical origin. Satellite imagery indicates that the cirrus were swept up from the southwest by a vigorous subtropical jet stream. Because these clouds were in a process of regeneration for a period of days as the convective anvil remnants were advected to mid-latitudes, their apparent impact on optics production must be related to the nature of the nuclei forming the cloud particles. In this way the source of the nuclei can have a lasting affect on the ice crystal properties as particles cyclically fall out of the layer and are replaced by newly generated ones from the reservoir of nuclei.

In contrast to most previous studies of cirrus particle formation, which appears to occur mostly through the homogeneous freezing of haze particles derived from cloud condensation nuclei composed of ammoniated salts, cloud condensation nuclei derived from the oceans' surface involve mainly chloride salts of sodium and magnesium. Current knowledge indicates that certain inorganic salts can strongly influence the morphology of ice crystals following nucleation because of the effects of electronic charge separations,[20] so it is possible that the changes in ice crystal shape induced by alkali halide solutions are effective at producing spectacular atmospheric optical displays. These pristine characteristics include solid, symmetric, and sharp-edged crystal forms. Certainly, in the few cases we have investigated, this appears to be the case.

Moreover, we point out that marine cloud condensation nuclei may also have a similar impact in that region of the globe that is known to generate the most abundant optical phenomena, the Antarctic polar plateau. In this case the lofting of the marine aerosol by strong convection is replaced by the gradual uplift of marine stratus clouds as they are swept up the plateau and cooled, until cloud droplet freezing occurs. An examination of the classic halo–arc photographs often reveals the presence of supercooled liquid stratus clouds on the horizon.[13]

This aircraft-supported case study was funded by U.S. National Aeronautics and Space Administration grant NAG5-6458 from the Earth Observing System program, U.S. National Science Foundation grant ATM-9528287, and U.S. Department of Energy grant DEFG02ER1059 from the Atmospheric Radiation

Measurement Program. The ray-tracing simulations were made possible by U.S. National Science Foundation grants ATM-9796277 and ATM-9907924. We thank P. Lawson for providing the *in situ* data.

References

1. R. A. R. Tricker, *Ice Crystal Haloes* (Atmospheric Optics Technical Group of the Optical Society of America, Washington, D.C., 1979), p. 30.
2. R. Greenler, *Rainbows, Halos, and Glories* (Cambridge U. Press, New York, 1980).
3. W. E. Parry, *Journal of a Voyage for the Discovery of a Northwest Passage* (1821), Reprint ed. (Greenwood, New York, 1968).
4. C. S. Hastings, "A general theory of halos," Mon. Weather Rev. **48,** 322–330 (1920).
5. A. Wegener, *Theorie der Haupthalos* (Archiv der Duetschen Seewarte 43, Hamburg, Germany, 1926).
6. P. Putnins, "Der bogen von Parry und andere beruhrungsbogen des gewohnlichen ringes," Meteorol. Z. **51,** 321–331 (1934).
7. K. Sassen, "Remote sensing of planar ice crystal fall attitudes," J. Meteorl. Soc. Jpn. **58,** 422–429 (1980).
8. K. Sassen, "Contrail-cirrus and their potential for regional climate change," Bull. Am. Meteorl. Soc. **78,** 1885–1903 (1997).
9. K. Sassen, "Lidar backscatter depolarization technique for cloud and aerosol research," in *Light Scattering by Nonspherical Particles: Theory, Measurements, and Geophysical Applications*, M. L. Mischenko, J. W. Hovenier, and L. D. Travis, eds. (Academic, New York, 2000), pp. 393–416.
10. S. Benson, "Lidar depolarization study to infer cirrus cloud microphysics," M.S. thesis (University of Utah, Salt Lake City, Utah, 1999).
11. K. Sassen, "Advances in polarization diversity lidar for cloud remote sensing," Proc. IEEE **82,** 1907–1914 (1994).
12. K. Sassen, "Cirrus clouds and haloes: a closer look," Opt. Photon. News **10,** 39–42 (1999).
13. W. Tape, *Atmospheric Halos*, Vol. 64 of Antarctic Research Series (American Geophysics Union, Washington, D.C., 1994).
14. Y. Takano and K. Jayaweera, "Scattering phase matrix for hexagonal ice crystals computed from ray optics," Appl. Opt. **24,** 3254–3263 (1985).
15. Y. Takano and K. N. Liou, "Solar radiative transfer in cirrus clouds. Part I: Single-scattering and optical properties of hexagonal ice crystals," J. Atmos. Sci. **46,** 3–19 (1989).
16. Y. Takano and K. N. Liou, "Halo phenomena modified by multiple scattering," J. Opt. Soc. Am. A **7,** 885–889 (1990).
17. R. P. Lawson, B. A. Baker, and C. G. Schmitt, "Microphysics of Arctic clouds observed during FIRE/ACE," J. Geophys. Res. (to be published).
18. K. Sassen, N. C. Knight, Y. Takano, and A. J. Heymsfield, "Effects of ice-crystal structure on halo formation: cirrus cloud experimental and ray-tracing modeling studies," Appl. Opt. **33,** 4590–4601 (1994).
19. K. Sassen, W. P. Arnott, J. M. Barnett, and S. Aulenbach, "Can cirrus clouds produce glories?," Appl. Opt. **37,** 1427–1433 (1998).
20. W. G. Finnegan and R. C. Pitter, "Ion-induced charge separations in growing single ice crystals: effects on growth and interaction processes," J. Colloid Interface Sci. **189,** 322–327 (1997).